

# Real-time Video-Based View Interpolation of Soccer Events using Depth-Selective Plane Sweeping

Patrik Goorts, Cosmin Ancuti, Maarten Dumont, Sammy Rogmans, Philippe Bekaert  
*Hasselt University - Expertise Centre for Digital Media, Wetenschapspark 2, 3590 Diepenbeek, Belgium*  
{patrik.goorts, cosmin.ancuti, maarten.dumont, sammy.rogmans, philippe.bekaert}@uhasselt.be

Keywords: Sports Broadcasting : View Interpolation : Plane Sweep : Virtual Viewpoint : Real-Time Processing

Abstract: In this paper we present a novel technique to synthesize virtual camera viewpoints for soccer events. Our real-time video-based rendering technique does not require a precise estimation of the scene geometry. We initially segment the dynamic parts of the scene to consequently estimate a depth map of the filtered foreground regions using a plane sweep strategy. The depth map is indicatively segmented to depth information per player. A consecutive plane sweep is used, where the depth sweep is limited to the depth range of each player individually, effectively removing major ghosting artifacts, such as third legs or ghost players. The background and shadows are interpolated independently. For maximum performance our technique is implemented using a combination of NVIDIA's shaders language Cg and NVIDIA's general purpose computing framework CUDA. The rendered results of an actual soccer game demonstrate the usability and accuracy of our framework.

## 1 Introduction

Nowadays, the demand for high-quality footage of sport events is higher than ever. Current caption systems therefore deliver high definition video in real-time. However, the viewpoints of these traditional systems are in general limited to the position of the physical cameras. In order to provide additional novel views from arbitrary positions in the scene, we develop a method that is able to synthesize virtual views in real-time. Compared with the traditional acquisition systems, our technique has the advantage to provide additional important features such as creating pleasant looking camera transitions, time freezing and interaction to the end users.

Our technique is a fully automatic real-time video-based method that generates images of virtual camera viewpoints, roughly placed in between physical cameras being demonstrated for a real soccer game. Video- and Image-based rendering techniques (IBR) represent a powerful alternative to geometry-based techniques to generate novel views. In contrast to accurately modeling the geometry, IBR techniques allow to visualize 3D environments using only the information of the captured images.

Our proposed method uses cameras with a fixed position in a semi-wide baseline setup, which is larger than a typical interpolation setup. In our framework, the dynamic parts (players) are first segmented and

consequently rendered independent from the background. Since we target a fast technique, a depth map of the filtered foreground regions is calculated using a plane sweep strategy. This initial depth map is employed to estimate the depth range of every player. Finally, the foreground is rendered using a depth-selective plane sweep, thus limiting the player-dependent depth range based on the previously calculated depth range of the foreground objects. This will provide a detailed depth map of every player without disturbing artifacts, while respecting its global depth. This novel interpolated image of the foreground is then merged with the interpolated background.

All algorithms are implemented using a combination of NVIDIA's Cg shader language and NVIDIA's general purpose computing framework CUDA and exploiting its interoperability. This combination allows for maximum performance by using the strengths of both frameworks and hiding the weaknesses (Rogmans et al., 2009b).

To demonstrate our method, we obtained video streams from a real soccer match using computer vision cameras placed approximately 1 meter apart from each other. Thanks to commodity graphics hardware and our parallel algorithmic approach, the interpolated view is obtained in real-time. The results show high-quality interpolation without typical interpolation artifacts, such as extra limbs, ghost players, distorted parallax effects or warping errors.

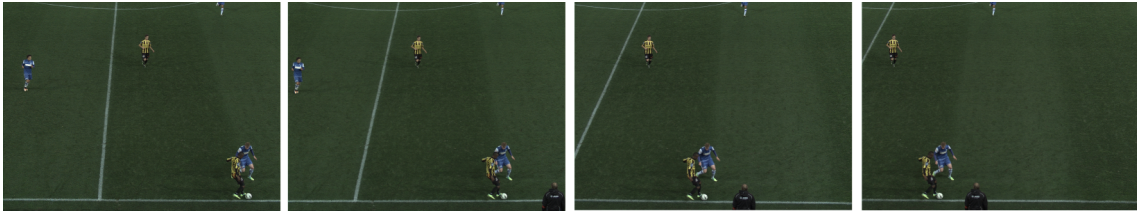


Figure 1: Examples of input images on positions 0, 1, 6 and 7

In Section 2, we will discuss the context of our work using related work. In Section 3, a detailed description of our setup is given. The prerendering phase of the method is elaborated in Section 4 and the real-time rendering phase in Section 5. Finally, the results are presented in Section 6, together with the conclusions in Section 7.

## 2 Related Work

To generate novel views, the existing methods are divided in two main classes: geometry-based rendering techniques and image-based rendering (IBR) techniques. When using geometry, the scene is reconstructed as a collection of 3D models. Visual hull (Matusik et al., 2000; Miller et al., 2005), photo hull (Kutulakos and Seitz, 2000) and space carving (Seitz and Dyer, 1999) are the most known strategies of this approach.

Some attempts transfer the studio-based reconstruction techniques for the outdoor sport events. One of these examples is the Eye vision system (eye, 2001) used to record the Super Bowl 2001 described in the work of Kanade et al. (Kanade et al., 1997). They used thirty motorized camera heads slaved to a single manually controlled camera to produce sweep shots with visible jumps between viewpoints. The framework of Hilton et al. (Hilton et al., 2011) reconstructs a 3D scene proxy at each frame starting with a volumetric reconstruction followed by a view-dependent refinement using information from multiple views.

On the other hand, image-based rendering techniques aim to visualize 3D scenes and objects in a realistic way by replacing the geometry and surface properties only with images. In contrast with geometry-based rendering techniques, IBR methods are more robust requiring more simpler and inexpensive setups. The most known approach is the generation of depth maps for small baseline setups using stereo matching (Seitz et al., 2006; Zitnick et al., 2004) and plane sweeping (Yang et al., 2004; Dumont et al., 2009), including depth-selective sweeping for two views (Rogmans et al., 2009a). Our method also belongs in the latter category of rendering techniques.



Figure 2: Overview of the camera setup. The setup consists of 8 computer vision cameras with 25mm lenses placed 1 meter apart from each other.

There have been several view interpolation systems that have been designed for soccer games. iView (Grau et al., 2007), commercialized by Red Bee Media (red, 2001), uses a narrow baseline camera setup and billboards or visual hulls to generate novel viewpoints of the soccer players. Shadow is synthetically applied to the result. However, some serious artifacts are reported when using the proposed methods, e.g. ghosting, flickering, missing limbs and blurred images.

Ohta et al. (Ohta et al., 2007) developed a technique that processes a simplified 3D model built on billboards. Hayashi and Saito (Hayashi and Saito, 2006; Inamoto and Saito, 2007) employ as well a billboard representation of dynamic regions while the interpolation is performed by estimating the projective geometry among different views. A similar method has been proposed recently by Germann et al. (Germann et al., 2010) that estimate the 2D pose using a database of silhouettes. Based on the pose and segmentation, the articulated billboard model is optimized in order to compensate for errors. Different than our approach, this technique requires manual intervention.

## 3 Framework Setup

To generate input video streams for our method, we created a setup consisting of an array of 8 Basler avA1600-50gc<sup>1</sup> computer vision cameras with 25mm

<sup>1</sup><http://www.baslerweb.com/products/aviator.html?model=204>

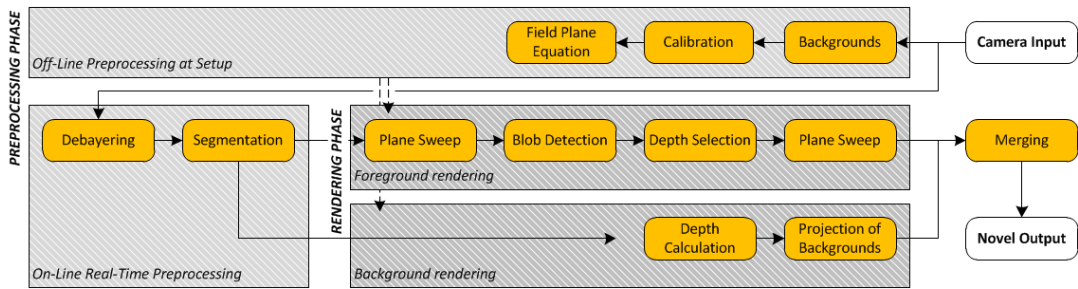


Figure 3: Overview of our method. There are two phases: a preprocessing phase, including calibration and background extraction, and a real-time rendering phase, where the foreground and the background are rendered independently.

lenses. The cameras are placed approximately 1 meter from each other, while the distance to the field is approximately 20 meters (see Figure 2). The cameras are triggered externally to provide global synchronization between the image streams. To provide high-quality results, the recording was done at 30 images per second with a resolution of  $1600 \times 1200$ . Figure 1 shows some example input images.

The raw images captured by the cameras  $C_i^r$  are transmitted to a rendering computer using a 10 Giga-bit Ethernet connection. The rendering computer allows to choose the location of a virtual camera  $C_v$  that, as will be described in the following, is processed in real-time. To acquire real-time processing, the computer is equipped with an NVIDIA GeForce GTX 580 running at 1544 MHz.

An overview of our method is shown in Figure 3. The method consists of two main phases: a preprocessing and a real-time rendering phase. These main tasks are discussed in the subsequent sections.

## 4 Preprocessing Phase

In the first step of our technique the camera positions are calibrated. This step is performed based on SIFT (Lowe, 2004) local feature points that are detected in the scene to generate camera correspondences. First, SIFT features are extracted from all input images  $C_i$ . Next, these features are matched between pairs of cameras using the k-d tree algorithm that searches similar features based on their closest distance. The pairwise correspondences are then tracked across multiple cameras using a graph-based search algorithm. The filtered matches are then used to calculate the position, orientation and the intrinsic parameters of the cameras based on the well-known techniques of Svoboda et al. (Svoboda et al., 2005). This method consists of hole-filling to deal with occlusions and a bundle adjustment with RANSAC. The invalid matches from the previous steps are removed

based on the RANSAC procedure.

Moreover, we calculate the position, represented as a plane equation, of the field. In our strategy this equation is acquired by manually selecting several matches (about 10 matches) on the field across all camera images  $C_i$  and using these matches to triangulate 3D points on the field. More correspondences, sparsely spread over the field, result in a more accurate estimation of the field. Afterwards, standard plane fitting is used to acquire the plane equation (Hartley and Zisserman, 2003), usable as a geometric representation of the field.

Furthermore, in this preprocessing step, backgrounds  $B_i$  are calculated using a per-pixel median filter. In order to provide a robust background generation, approximately 30 images are captured at a rate of 2 frames per minute right before the actual recording. When the lighting changes in the scene, it might be required to repeat this procedure during the processing using a subset of the captured images.

## 5 Real-time Rendering Phase

Our real-time rendering phase consists of four parts: frame preprocessing, background rendering, foreground rendering and merging.

### 5.1 Frame Preprocessing

When running the setup, every acquired frame must be preprocessed before the actual rendering step. These steps include debayering and segmentation.

Firstly, the raw input images  $C_i^r (i \in [1, N])$  need to be debayered. The cameras provide raw images, where every pixel only contains the value of one color channel. The color is defined by the specific color pattern used in the camera sensor, i.e. the Bayer pattern. The values of the other color channels of the pixel are interpolated using the surrounding pixel values. This is done by uploading the raw image

to the GPU and applying the AHD method of Hirakawa and Parks (Hirakawa and Parks, 2005), coded in NVIDIA's shader language Cg. By using our own GPU implementation of debayering, we avoid uncontrolled and lower quality processing on camera hardware, reduce the amount of camera-computer data copying with a factor three, and therefore increase the arithmetic intensity of the GPU by making the results locally available for the subsequent algorithms.

Secondly, the debayered images  $C_i$  are segmented on the GPU using the backgrounds  $B_i$  of the pre-rendering step. To provide real-time processing, the segmentation is processed on a pixel basis and uses thresholds  $\tau_f, \tau_b, \tau_a$ , with  $\tau_f > \tau_b$ :

$$s_i = \begin{cases} 1: & \tau_f < \|c_i - b_i\| \\ 1: & \tau_f \geq \|c_i - b_i\| \geq \tau_b \text{ and } \cos(\widehat{c_i b_i}) \leq \tau_a \\ 0: & \|c_i - b_i\| < \tau_b \\ 0: & \tau_f \geq \|c_i - b_i\| \geq \tau_b \text{ and } \cos(\widehat{c_i b_i}) > \tau_a \end{cases} \quad (1)$$

with  $s_i = S_i(x, y)$ ,  $c_i = C_i(x, y)$  and  $b_i = B_i(x, y)$ , for all pixels  $(x, y)$ .  $\widehat{c_i b_i}$  is the angle between the foreground and background color. We measure the difference between the foreground and background pixels. When the difference is large (larger than  $\tau_f$ ), the pixel is considered as foreground. If the difference is small (smaller than  $\tau_b$ ), the pixel is considered as background. When the difference is in between these thresholds, we consider the vector angle between the colors and apply the threshold  $\tau_a$ . Finally, the segmentation is enhanced with an erosion and dilation step to reduce small segmentation errors caused by noise in the input streams (Yang and Welch, 2002).

The thresholds should be chosen such that the foreground objects, like players and the ball, are considered as foreground, but the shadows are considered as background. The shadows are in essence a darker background, while foregrounds do not correlate with the background, thus allowing the use of thresholds. We do not consider shadow as foreground to reduce interpolation artifacts caused by mismatches in shadow regions. Shadows are located on the background, thus eliminating the need for separate interpolation; the shadows are interpolated together with the background.

After these preprocessing steps, the background  $B_v$  and foreground  $F_v$  of the virtual view are rendered independently.

## 5.2 Background Rendering

To generate the background  $B_v$  of the virtual image, we take the input images  $C_i$  and replace the foreground pixels with the values from the background

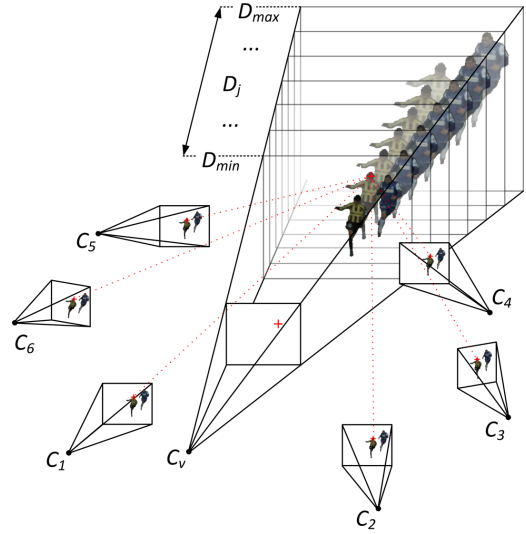


Figure 4: Principle of plane sweeping. The space before the virtual camera  $C_v$  is discretized in planes. For every depth  $D_j$ , every pixel of the virtual view is deprojected on this plane and back projected on every input camera  $C_1 - C_6$ . Using these color values, a cost error  $\epsilon$  can be calculated, thus deriving the optimal depth for that virtual pixel.

images  $B_i$ , according to the segmentation. This will preserve the shadows of the objects, while removing foreground pixels which can cause artifacts.

These generated frame backgrounds are then projected and blended on the plane as determined in the preprocessing phase. The projection is dependent of the parameters of the input cameras and the parameters of the current virtual view and should be repeated for every frame.

## 5.3 Initial Plane Sweeping

The foreground  $F_v$  is rendered in three passes. First, a global plane sweep is performed to generate a crude depth map and segmentation of the virtual viewpoint. Our plane sweep is an adopted and modified version of the well-known method from Yang et al. (Yang et al., 2003). The world before the virtual camera is divided in  $M$  planes of depths  $D_p \in [D_{min}, D_{max}]$ , parallel to the virtual image plane, as can be seen in Figure 4. For every plane, every pixel  $v(x, y)$  of the virtual camera image is deprojected on this plane, reprojected on the input images and the error  $\epsilon$  is calculated per pixel and per depth plane using the sum of squared differences (SSD):

$$\epsilon = \sum_{i=1}^N \frac{\|\gamma - C_i\|^2}{3N} \text{ with } \gamma = \sum_{i=1}^N \frac{C_i}{N} \quad (2)$$

where  $\gamma$  is the average of the reprojected pixels and



Figure 5: Final results of the method for a frozen frame. The positions are 0.5, 3.5 and 6.5.

$C_i$  is the  $i^{\text{th}}$  input image of total  $N$ . When a reprojected pixel falls outside the segmentation mask, the error  $\epsilon$  for that depth is set to infinity. This will guarantee consistency with the segmentation. The resulting depth  $d_l$  for a virtual pixel is the depth plane on depth  $D_l$  with the lowest error  $\epsilon$  for that virtual pixel, and the color is the average  $\gamma$  of the corresponding pixels in the input images. When every  $\epsilon$  is infinity, the pixel in the virtual image is considered as background. The calculation of the depth map and the resulting color image can efficiently be implemented using Cg on graphics hardware by exploiting the projective texturing capabilities, resulting in real-time processing (Dumont et al., 2009).

#### 5.4 Depth Selection

After the initial plane sweep, we select a depth range per player visible in the virtual view. The depth map is split up in unconnected blobs of pixels. These represent an independent player or a group of players. This is achieved using a parallel region growing algorithm created for CUDA (Ziegler and Rasmusson, 2010). Initially, every pixel is assigned an unique label. Next, we assign one thread per pixel. Every thread will compare the label of its neighboring pixels with its own label and will assign the lowest of the two to itself. Neighboring pixels that originate from the background are ignored. This process is repeated until no more changes are made. Now every foreground pixel has a label that is the same as every other connected pixel. Pixels with the same label form one distinct blob or foreground object. Every detected object is then filled with the median of the depth values of that object. This depth represents the global depth  $d_l$  of the player (or group of players) in that foreground object. CUDA is used to harness the utilization of a user-managed cache, allowing more efficient memory management than can be obtained by normal texture lookups (Goorts et al., 2009). By exploiting the interoperability of Cg and CUDA, no performance penalty is perceived.

#### 5.5 Depth-Selective Plane Sweeping

Finally, this filtered depth map is used in a second “depth-selective plane sweep”, extending the stereo principle of Rogmans et al. (Rogmans et al., 2009a). While sweeping over the range of depth values  $D_p \in [D_{min}, D_{max}]$ , only values within a certain fraction  $\alpha$  of the depths  $d_l$  calculated in the previous step are accepted if the following expression is satisfied:

$$|D_p - d_l| < \alpha(D_{max} - D_{min}) \quad (3)$$

Depths that are not accepted are explicitly assigned an error  $\epsilon$  of infinity. If every error is infinity, the virtual pixel will be considered as background, removing artifacts caused by mismatching.

This assures a detailed depth map of the player, while respecting its global depth. Extra limbs and other ghosting artifacts are filtered out using this method. Indeed, these arise from errors in the matching process of the first plane sweep. For example, the left leg of one player is matched to his right leg, resulting in a third leg in the virtual view (this can be seen in Figure 7 (a)). However, the depth of this ghost leg is distinct from the depth of the correct pixels of the player. Using our method, this depth is filtered out and the ghost leg is considered as background. Small artifacts due to errors in the reprojection are reduced by limiting the depth range per player, thus obtaining a high quality depth map without large errors in the individual depth values.

While the former method will remove many artifacts, some artifacts can not be eliminated. Errors in the matching process can result in the manifestation of ghost players, i.e. when one player of one camera image matches to another player in another camera. However, in our experiments this rarely happens due to our segmentation constraints. The depth filtering will not eliminate these artifacts, because these are disconnected from other desirable blobs of players. Therefore, we also consider the depth of the background and remove every pixel where the depth deviates more than a certain range  $\beta$  from the depth of the

background on that pixel. Because the background is a plane and the foreground is related to the background, this method will effectively filter out extreme mismatches in the foreground.

## 5.6 Merging

The rendering of the foreground  $F_v$  and background  $B_v$  are then merged using the segmentation obtained from the second plane sweep. To generate a pleasant-looking result, the borders of the foreground are slightly feathered and blended with the background.

## 6 Results

Figure 5 shows interpolated views of a frozen frame. Figures 6, 7 and 8 show some detailed results of our method for different scenes. Figure 6a, 7a and 8a show the resulting depth map of normal plane sweeping. These depth maps contain significant noise and artifacts, which reduce the quality of the final results.

The first filtering process applied in our strategy consists of filtering the depth values per connected blobs of pixels, as explained in Subsection 5.3. We fixed the parameters of the method for every result on 0.01 for  $\alpha$  and 0.2 for  $\beta$ . Figure 6b and 7b show the depth map after foreground object detection and calculating the median per object. Notice that only the depth values are altered and artifacts (like a ghost leg in Figure 7b) are still present. However, these artifacts now have a very different depth value than the original value. The final depth maps and the results after the depth-selective plane sweep are shown in Figure 6c-d and 7c-d. Notice that after the filtering stage the results are sharp and no visible artifacts are present.

Figure 8a and 8e show artifacts that can not be removed with this filtering strategy. Here, an artifact is visible in between the two players and is not filtered out after the second plane sweep, as can be seen in Figure 8b. When we use the depth information (Figure 8c) of the background and remove every blob where the depth value differs too much, we are able to remove these artifacts also, as can be seen in Figure 8d.

By using depth filtering, we effectively remove large artifacts. The small artifacts, such as wrong colors by reprojection errors, are removed due to the high quality depth map obtained by the depth-selective plane sweep.

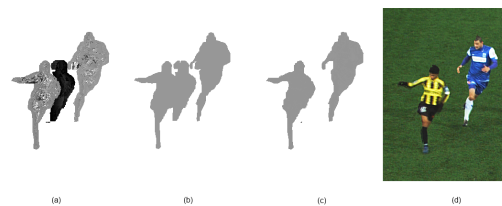


Figure 6: Detail of the method: (a) Depth map of standard plane sweep. (b) Filtered depth. (c) Depth map of the depth-selective plane sweep. The artifacts are effectively removed. (d) Final merged result.

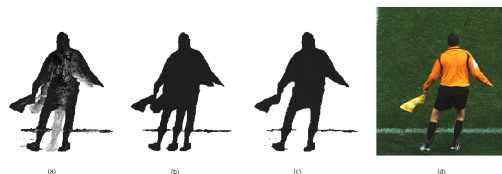


Figure 7: Detail of the method: (a) Depth map of standard plane sweep. (b) Filtered depth. (c) Depth map of the depth-selective plane sweep. The ghost leg and other artifacts are effectively removed. (d) Final merged result.

## 7 Conclusions

In this paper, we presented a new method to acquire interpolated views from a soccer game for physical cameras in a semi-wide baseline setup. We firstly estimate the depth of every player and then refine this depth, which allows the generation of a high quality interpolated view of the players. The background and shadows are generated separately using a geometry-based interpolation. The main advantage of our technique is that the entire pipeline is implemented using graphics hardware, which allows real-time processing and interpolation. A one-time camera calibration and background generation step is required at setup.

The results show that the method yields high-quality results without disturbing ghosting artifacts, parallax errors, etc., which most image-based algorithms suffer from.

## 8 Acknowledgments

Patrik Goorts would like to thank the IWT for its PhD specialization bursary.

## REFERENCES

- (2001). 3d graphics systems by red bee media. <http://redbeemedia.com/html/live-graphic.html>.
- (2001). Eye vision at the super bowl. <http://www.ri.cmu.edu/events/sb35/tksuperbowl.html>.

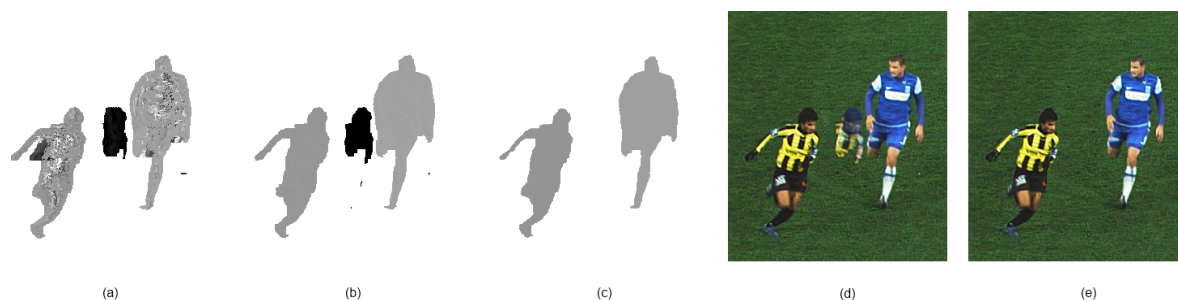


Figure 8: Detail of the method: (a) Depth map of standard plane sweep. (b) Filtered depth map after the depth-selective plane sweep. Not all artifacts are removed. The depth of the artifact differs a lot from the depth of the background. (c) Depth after the depth-selective plane sweep after the removal of the artifact. (d) Result without filtering using the background depth. (e) Result with filtering using the background depth.

- Dumont, M., Rogmans, S., Maesen, S., and Bekaert, P. (2009). Optimized two-party video chat with restored eye contact using graphics hardware. *e-Business and Telecommunications*, pages 358–372.
- Germann, M., Hornung, A., Keiser, R., Ziegler, R., Würmlin, S., and Gross, M. (2010). Articulated billboards for video-based rendering.
- Goorts, P., Rogmans, S., and Bekaert, P. (2009). Optimal Data Distribution for Versatile Finite Impulse Response Filtering on Next-Generation Graphics Hardware using CUDA. In *Proc. of The Fifteenth Intl. Conference on Parallel and Distributed Systems*, pages 300–307.
- Grau, O., Hilton, A., Kilner, J., Miller, G., Sargeant, T., and Starck, J. (2007). A Free-Viewpoint Video System for Visualization of Sport Scenes. *SMPTE motion imaging journal*, 116(5/6):213.
- Hartley, R. and Zisserman, A. (2003). *Multiple view geometry in computer vision*, volume 2. Cambridge Univ Press.
- Hayashi, K. and Saito, H. (2006). Synthesizing Free-Viewpoint Images from Multiple View Videos in Soccer Stadium. In *Intl. Conf. on Computer Graphics, Imaging and Visualisation*, pages 220–225.
- Hilton, A., Guillemot, J., Kilner, J., Grau, O., and Thomas, G. (2011). 3d-tv production from conventional cameras for sports broadcast. *IEEE Transactions on Broadcasting*, (99):1–1.
- Hirakawa, K. and Parks, T. (2005). Adaptive homogeneity-directed demosaicing algorithm. *Image Processing, IEEE Transactions on*, 14(3):360–369.
- Inamoto, N. and Saito, H. (2007). Virtual viewpoint replay for a soccer match by view interpolation from multiple cameras. *IEEE Transactions on Multimedia*, 9(6):1155–1166.
- Kanade, T., Rander, P., and Narayanan, P. (1997). Virtualized reality: Constructing virtual worlds from real scenes. *Multimedia, IEEE*, 4(1):34–47.
- Kutulakos, K. and Seitz, S. (2000). A theory of shape by space carving. *Intl. Journal of Computer Vision*, 38(3):199–218.
- Lowe, D. (2004). Distinctive image features from scale-invariant keypoints. *Intl. journal of computer vision*, 60(2):91–110.
- Matusik, W., Buehler, C., Raskar, R., Gortler, S., and McMillan, L. (2000). Image-based visual hulls.
- Miller, G., Hilton, A., and Starck, J. (2005). Interactive free-viewpoint video.
- Ohta, Y., Kitahara, I., Kameda, Y., Ishikawa, H., and Koyama, T. (2007). Live 3D Video in Soccer Stadium. *Intl. Journal of Computer Vision*, 75(1):173–187.
- Rogmans, S., Dumont, M., Cuypers, T., Lafruit, G., and Bekaert, P. (2009a). Complexity reduction of real-time depth scanning on graphics hardware.
- Rogmans, S., Dumont, M., Lafruit, G., and Bekaert, P. (2009b). Migrating real-time depth image-based rendering from traditional to next-gen gpgpu.
- Seitz, S., Curless, B., Diebel, J., Scharstein, D., and Szeliski, R. (2006). A comparison and evaluation of multi-view stereo reconstruction algorithms.
- Seitz, S. and Dyer, C. (1999). Photorealistic scene reconstruction by voxel coloring. *Intl. Journal of Computer Vision*, 35(2):151–173.
- Svoboda, T., Martinec, D., and Pajdla, T. (2005). A convenient multicamera self-calibration for virtual environments. *Presence: Teleoperators & Virtual Environments*, 14(4):407–422.
- Yang, R., Pollefeys, M., Yang, H., and Welch, G. (2004). A unified approach to real-time, multi-resolution, multi-baseline 2d view synthesis and 3d depth estimation using commodity graphics hardware. *Intl. Journal of Image and Graphics*, 4(4):627–651.
- Yang, R. and Welch, G. (2002). Fast image segmentation and smoothing using commodity graphics hardware. *Journal of graphics tools*, 7(4):91–100.
- Yang, R., Welch, G., and Bishop, G. (2003). Real-time consensus-based scene reconstruction using commodity graphics hardware.
- Ziegler, G. and Rasmusson, A. (2010). Efficient volume segmentation on the gpu.
- Zitnick, C., Kang, S., Uyttendaele, M., Winder, S., and Szeliski, R. (2004). High-quality video view interpolation using a layered representation.